







## RESEARCH ARTICLE

# Examining the contact problem of a functionally graded layer supported by an elastic half-plane with the analytical and numerical methods

Murat Yaylacı<sup>1,2,3</sup>  | Müjgen Yaylı<sup>1</sup> | Şevval Öztürk<sup>1</sup>  | Sevil Ay<sup>4</sup>  |  
Mehmet Emin Özdemir<sup>5</sup>  | Ecren Uzun Yaylacı<sup>6</sup>  | Ahmet Birinci<sup>7</sup> 

<sup>1</sup>Department of Civil Engineering, Recep Tayyip Erdogan University, Rize, Turkey

<sup>2</sup>Turgut Kıran Maritime Faculty, Recep Tayyip Erdogan University, Rize, Turkey

<sup>3</sup>Murat Yaylacı-Luzeri R&D Engineering Company, Rize, Turkey

<sup>4</sup>Department of Civil Engineering, Artvin Coruh University, Artvin, Turkey

<sup>5</sup>Department of Civil Engineering, Cankiri Karatekin University, Çankırı, Turkey

<sup>6</sup>Faculty of Engineering and Architecture, Recep Tayyip Erdogan University, Rize, Turkey

<sup>7</sup>Department of Civil Engineering, Karadeniz Technical University, Trabzon, Turkey

## Correspondence

Murat Yaylacı, Murat Yaylacı-Luzeri R&D Engineering Company, 53100, Rize, Turkey.

Email: [murat.yaylaci@erdogan.edu.tr](mailto:murat.yaylaci@erdogan.edu.tr)

This study offers a comparative study of the analytical and numerical methods for investigating a contact problem. The contact problem comprises a functionally graded layer supported by a half-plane and loaded with a distributed load from the top surface. First, the analytical and numerical solutions to the problem are acquired by utilizing a theory of elasticity and finite element method, respectively. The problem is transformed into a system of integral equations in which the contact stress is an unknown function. The solution of the integral equation was achieved with Gauss–Jacobi integration formulation. The finite element model of the problem is created using ANSYS software, and the two-dimensional analysis of the problem is performed. Results were obtained from the samples for different material properties and loading conditions. The distributed load width and non-homogeneity parameters significantly impact on contact mechanics. The results indicate that the contact area and the contact stress obtained from finite element method (FEM) are close to the analytical results. As a result, acceptable error rates were obtained. Finally, this study provides evidence of a good agreement between the two methods.

## KEYWORDS

contact problem, finite element method, functionally graded layer, theory of elasticity

## MSC CLASSIFICATION

00A05, 00A69, 45-xx, 35A22, 74B05, 26B20, 74S05

## 1 | INTRODUCTION

The subject of contact mechanics has an essential place in mechanical and civil engineering, and it has become increasingly popular, especially in the last 30 years. It is accepted that contact mechanics emerged with the article “On the contact of elastic solids,” written by Heinrich Herz in 1882. Basically, contact mechanics is the study of problems to determine, explain, or define the damage and shaping methods [1].

This is an open access article under the terms of the [Creative Commons Attribution](https://creativecommons.org/licenses/by/4.0/) License, which permits use, distribution and reproduction in any medium, provided the original work is properly cited.

© 2024 The Authors. *Mathematical Methods in the Applied Sciences* published by John Wiley & Sons Ltd.

In this direction, the application areas of contact mechanics include the primary engineering fields such as foundations, railways, highways, airport superstructures, cylindrical shafts, and shafts, as well as the behavior of human joints and biomechanics, including prosthesis and implant issues. Heinrich Hertz studied the balance of two elastic bodies in contact, assuming that the contact zone is elliptical, and developed a formulation for contact stress and strains. In layered materials, the sudden change of material properties on the bonding surface can damage the materials in contact beginning from the bonding surface and cause the materials to separate from each other over time. To prevent this problem, a new material class, Functionally Graded Materials (FGMs), has emerged in engineering applications. FGMs are heterogeneous composite materials in which material properties may differ from one surface to another on the material, depending on a defined function. In particular, the necessity of a homogeneous material that provides high strength to spacecraft, is resistant to thermal effects, and exhibits thermal resistance has increased the orientation to the field of FGM, which can combine these features. Due to their ability to reduce surface tensions, FGMs have had various applications, such as mechanical, electronics, chemical engineering, aerospace, energy, optical materials, and biomedical engineering, since their emergence [2–8].

Contact mechanics is an important research topic for many researchers. Researchers approach the solution of different types of contact problems with two methods: analytical and numerical. In addition to these two methods, there are also problems created with layers containing FGM. For this reason, contact problems examined using analytical and numerical analysis methods in the literature occupy an extensive area [9–16].

Some studies in the literature that solve FGM problems analytically are listed below. Muskhelishvili (1953) and England (1971) used the analytical continuation method based on the theory of complex variables to solve pressure problems [17, 18]. After the method, the general solution of the pressure problem is made by the reduction method to the linear equation system that can be expressed with the basic Plamelj function. Adams (1978) used the theory of elasticity to examine the behavior of an elastic layer sitting on a semi-infinite plane under the effect of a single moving load. As a result of the study, the contact stresses were determined, as well as the location and size of the contact zone for various material properties and velocity magnitudes [19]. Saito and Terasawa (1980) investigated the vibration of an infinite beam supported by a Pasternak foundation and under the effect of a moving load. They obtained the equations of motion using the theory of elasticity and the solution using the Fourier transform. The results were compared with those obtained from the Timoshenko and Bernoulli-Euler beam theorems [20]. Dempsey et al. (1990) investigated the contact problem of an infinitely long elastic layer based on Winkler under different loadings. Different loading cases acting on the layer were solved separately according to elasticity and beam theory, and the results obtained were compared [21]. Giannakopoulos and Suresh (1997) investigated the contact stresses in axisymmetric functionally graded materials loaded with frictionless flat, conical, and spherical rigid blocks [22]. Chao and Gao (2000) used the analytical continuation method to solve a problem created for a thermoelastic half-plane with a rigid punch of various shapes. As a result of the study, the effects of applied loads, punch profile, and material properties on the contact stress under the punch face were examined in detail [23]. Güler and Erdoğan (2004) studied the contact problem in graded coatings limited by homogeneous substrates loaded with rigid thrusts in triangular and rectangular profiles [24]. Ke and Wang (2006) investigated the contact problem when friction forces act perpendicularly by applying a singular force with an elastic punch to an elastic half-plane covered with a thin layer [25]. Yang and Ke (2008) investigated the frictionless contact problem for a tripartite structure consisting of a pavement layer, a Functionally Graded (FG) layer, and a substrate under a rigid cylindrical block. The coating layer and the substrate are homogeneous materials with different physical properties. The intermediate layer is FGM, and the shear modulus varies arbitrarily throughout the thickness [26]. Aizikovitch et al. (2011) developed an analytical method that efficiently solves contact problems in materials with properties that vary arbitrarily across depth [27]. Volkov et al. (2013) investigated the contact problem in the case of the FG elastic layer loaded with a circular block, in line with the approximate analytical solution method [28]. Yan and Li (2015) investigated the frictionless separation contact problem between an FG layer and an elastic layer, accepting that the FG layer is isotropic and the shear modulus of the layer varies depending on an exponential function along the thickness [29]. In addition to the summarized studies above, the literature also includes studies evaluating layered structures' behavior under different wave types outside the contact problem [30–36].

Numerical methods, one of the methods of solving contact problems, have led to the development of studies in this field in line with the technological developments in recent years. Methods such as integral transformation techniques, finite differences, and finite elements can be examples of these studies. The finite element method is important in solving contact problems in terms of allowing the relationship of elements in a particular geometry to each other, the mechanical and physical properties of materials, and the definition of complex boundary conditions [37–46].

In the literature, many studies on contact problems are solved using the finite element method. Schwarzer et al. (1995) solved the contact problem in a laminated layer with a notch analytically and numerically [47]. Güler et al. (2012) presented a two-dimensional analytical solution that can be applied to three-dimensional problems with its adaptability for plane stress and plane strain geometries. The study used the determined analytical formulation as a basis for validating the finite element results [48]. Abhilash and Murthy (2014) determined the two-dimensional elastic contact of a semi-infinite plane covered with FGM and loaded with a punch using the finite element method [49]. Liu et al. (2018) examined the contact problem of two bonded layers sitting on a half-plane. The study assumed the system was homogeneous on the top layer and FGM on the bottom. The problem was solved analytically and numerically, and the results were compared [50].

According to the literature, the FG layer's shear modulus varies based on an exponential function. In general, how the material stiffness parameter affects the contact stresses and contact region length has been researched. However, the difference in the problem geometry, loading, and geometry that are applied distinguishes this research from other studies of a similar nature in the literature. This research used the analytical solution based on the theory of elasticity (ET) and the numerical solution based on the finite element method (FEM) to investigate the frictionless and detached contact mechanics of the FG layer resting on an elastic half-plane (HP) under two symmetrical distributed loads. For the different dimensionless quantities, dimensionless contact stresses between the FG layer and half plane were determined. The results of each of these methods were compared with one another.

## 2 | THEORETICAL APPROACH (THEORY OF ELASTICITY)

### 2.1 | Definition of the problem

In this part, the frictionless contact problem of the FG layer supporting the elastic HP is investigated depending on the theory of elasticity. Figure 1 presents the geometry and loading cases of the problem. The FG layer's shear modulus changes depending on an exponential function along the layer height, as given in Equation (1). It is supposed that the shear module of the HP is the same everywhere, that is, homogeneous.

$$\mu_1(y) = \mu_0 e^{\beta y}, \quad (0 \leq y \leq h) \quad (1)$$

The expressions in the figure and equation are defined as follows.

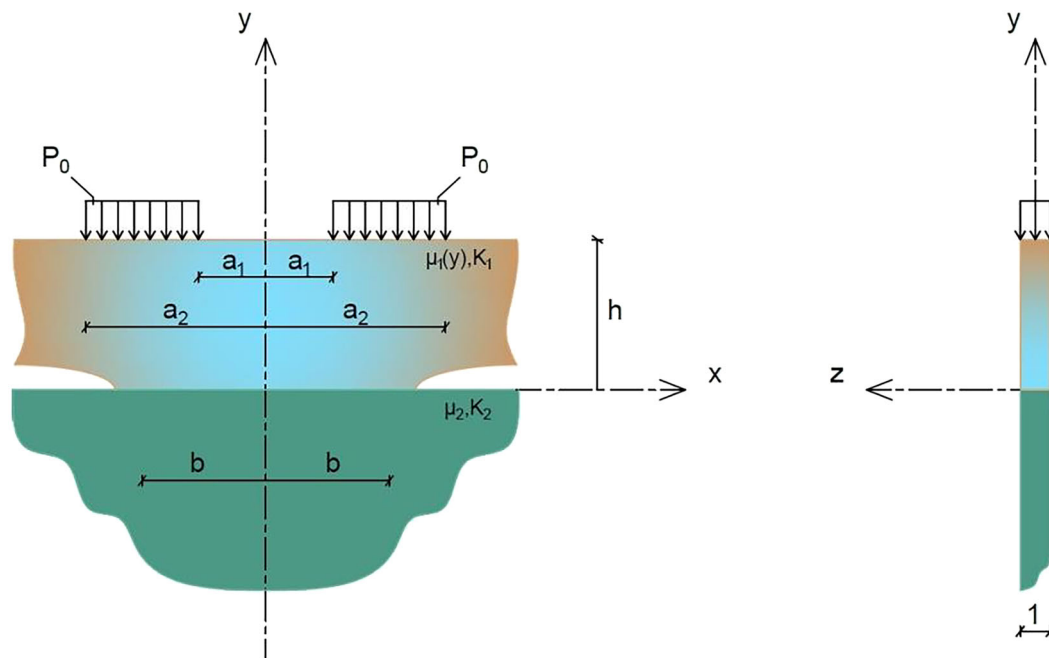


FIGURE 1 Definition of the problem. [Colour figure can be viewed at [wileyonlinelibrary.com](http://wileyonlinelibrary.com)]

- $\mu_2$ : The shear modulus of the HP.
- $\mu_1$ : The shear modulus of the FG layer.
- $\mu_0$ : The shear modulus on the lower surface of the FG layer.
- $\beta$ : The non-homogeneity parameter ( $\beta \neq 0$ ).
- $\nu_1$ : The Poisson constant of the FG layer.
- $\nu_2$ : The Poisson constant of the HP.
- $a_2$ - $a_1$ : The distributed load length.
- $b$ : Contact distance between FG layer and HP.
- $h$ : The height of the FG layer.

The HP is homogeneous and has a constant shear modulus. The FG layer's top surface is under two symmetrical distributed loads. It is assumed that contact between all surfaces is frictionless, and the effect of gravity force is neglected. Thickness in the  $z$ -direction is taken to be a unit.

In the problem equations, (1) indexed expressions belong to the FG layer and (2) indexed expressions belong to the HP. Displacement and stress relations used in the solution of the problem can be written for the FG layer and elastic half plane as follows:

For FG layer displacement and stress expressions:

$$u_1(x,y) = \frac{2}{\pi} \int_0^{\infty} \sum_{j=1}^4 A_j e^{n_j y} \sin(\xi x) d\xi \quad (2)$$

$$v_1(x,y) = \frac{2}{\pi} \int_0^{\infty} \sum_{j=1}^4 A_j m_j e^{n_j y} \cos(\xi x) d\xi$$

$$\sigma_{1x} = \frac{2\mu_0 e^{\beta y}}{\pi(\kappa_1 - 1)} \int_0^{\infty} \sum_{j=1}^4 A_j [(3 - \kappa_1) m_j n_j + \xi(\kappa_1 + 1)] e^{n_j y} \cos(\xi x) d\xi \quad (3)$$

$$\sigma_{1y} = \frac{2\mu_0 e^{\beta y}}{\pi(\kappa_1 - 1)} \int_0^{\infty} \sum_{j=1}^4 A_j C_j e^{n_j y} \cos(\xi x) d\xi$$

$$\tau_{1xy} = \frac{2\mu_0 e^{\beta y}}{\pi} \int_0^{\infty} \sum_{j=1}^4 A_j D_j e^{n_j y} \sin(\xi x) d\xi$$

For elastic FG layer displacement and stress expressions:

$$u_2(x,y) = \frac{2}{\pi} \int_0^{\infty} [(B_1 + B_2 y) e^{\xi y}] \sin(\xi x) d\xi \quad (4)$$

$$v_2(x,y) = \frac{2}{\pi} \int_0^{\infty} \left[ \left[ -B_1 + \left( \frac{\kappa_2}{\xi} - y \right) B_2 e^{\xi y} \right] \right] \cos(\xi x) d\xi$$

$$\frac{1}{2\mu_2} \sigma_{2x}(x,y) = \frac{2}{\pi} \int_0^{\infty} \left[ \xi(B_1 + B_2 y) + \left( \frac{3 - \kappa_2}{2} \right) B_2 \right] e^{\xi y} \cos(\xi x) d\xi \quad (5)$$

$$\frac{1}{2\mu_2} \sigma_{2y}(x,y) = \frac{2}{\pi} \int_0^{\infty} \left[ -\xi(B_1 + B_2 y) + \left( \frac{1 + \kappa_2}{2} \right) B_2 \right] e^{\xi y} \cos(\xi x) d\xi$$

$$\frac{1}{2\mu_2} \tau_{2xy}(x,y) = \frac{2}{\pi} \int_0^{\infty} \left[ \xi \left( B_1 + B_2 y \right) + \left( \frac{1 - \kappa_2}{2} \right) B_2 \right] e^{\xi y} \sin(\xi x) d\xi$$

where  $\mu_i(x,y)$  and  $\nu_i(x,y)$  are the  $x$  and  $y$  components of the displacement vector and  $\sigma_x(x,y)$ ,  $\sigma_y(x,y)$ ,  $\tau_{xy}(x,y)$  are the stress components of the layers.  $\kappa_i = (3-4\nu_i)\kappa_i = (3-4\nu_i)$  for plane strain and  $\nu_i$  is the Poisson's ratio.  $A_j$  ( $j = 1,2,3,4$ ),  $B_1$ , and  $B_2$  are the unknown coefficients for the layers, which will be determined from the boundary conditions of the problem.

Boundary conditions of the contact problem can be written as

Boundary conditions:

$$\sigma_{y1}(x, h) = \begin{cases} -p_0; & a_1 < x < a_2 \\ 0; & x > a_2 \text{ or } x < a_1 \end{cases} \quad (6)$$

$$\tau_{xy1}(x, h) = 0, \quad (0 \leq x < \infty)$$

$$\sigma_{y2}(x, 0) = \begin{cases} -p_1(x); & 0 \leq x < b \\ 0; & b \leq x < \infty \end{cases}$$

$$\sigma_{y1}(x, 0) = \sigma_{y2}(x, 0), \quad (0 \leq x < \infty)$$

$$\tau_{xy1}(x, h) = 0, \quad (0 \leq x < \infty)$$

$$\tau_{xy2}(x, h) = 0, \quad (0 \leq x < \infty)$$

$$\frac{\partial}{\partial x} [\nu_1(x, 0) - \nu_2(x, 0)], \quad (0 \leq x < b) \quad (7)$$

Equilibrium conditions of the problem may be expressed as

$$\int_{-b}^b p_1(x) dx = 2(a_2 - a_1)p_0 \quad (8)$$

where  $p_0$  is a known distributed load, and  $p_1(x)$  is the unknown contact pressures on the contact areas ( $b$ ).  $a_1$  and  $a_2$  represent the starting and ending points of the distributed load, respectively.

The solution of the system of the integral equations.

By using boundary Conditions (6),  $A_j$  ( $j = 1,2,3,4$ ),  $B_1$  and  $B_2$  coefficients can be determined in terms of  $p_1(x)$  (Appendix A). After some routine manipulations and using the symmetry conditions  $p_1(x) = p_1(-x)$ , one may obtain the following system of singular integral equation.

$$p_0 M(x) + \frac{2}{\pi} \int_{-b}^b P_1(t) \left\{ k(x, t) + \left[ \frac{1}{t-x} \right] \left[ \frac{\kappa_1 + 1}{8\mu_0} + \frac{\kappa_2 + 1}{8\mu_2} \right] \right\} dt = 0 \quad (9)$$

where  $M(x)$ ,  $k(x, t)$  and  $\Delta$  are explained in Appendix B.

The numerical solutions of the integral equations will be achieved by Gauss-Jacobi Integration Formulation, which is given in the studies of Erdogan et al. (1973) and Krenk (1975) [51, 52]. The following dimensionless quantities can be introduced to simplify the numerical analysis of the integral equation.

$$z = \xi h, \quad dz = h d\xi, \quad x = bs, \quad t = br, \quad dt = bdr \quad (10)$$

$$\phi(r) = \frac{h}{P} P_1(t) \quad (11)$$

Substituting these dimensionless quantities given in (10) into (8) and (9), these equations may be written as follows

$$\int_{-1}^1 \phi(r) \left\{ \frac{b}{h} k(s, r) + \left[ \frac{1}{r-s} \right] \left[ \frac{\kappa_1 + 1}{8} + \frac{\mu_0(\kappa_2 + 1)}{8\mu_2} \right] \right\} dr = -\frac{p_0}{p/h} M(s) \quad (12)$$

$$\frac{b}{h} \int_{-1}^1 \phi(r) dr = (a_2 - a_1) \frac{p_0}{p} \quad (13)$$

One may notice that because of the smooth contact at the endpoint  $b$ , the unknown function  $p_i(x)$  is zero at the ends; thereby, the index of the integral Equation (12) is “−1”. Its solution may be expressed as Erdoğan and Gupta (1972) [53].

$$g_j(r_j) = G_j(r_j) w_j(r_j), w_j(r_j) = (1 - r_j)^{\alpha_j} (1 + r_j)^{\beta_j}, j = 1, 2 \quad (14)$$

Using the Gauss–Jacobi integration formulas, the integral Equation (12) and equilibrium Conditions (13) become

$$\sum_{i=1}^N W_i g(r_i) \left[ \left\{ \frac{b}{h} k(s_k, r_i) + \left[ \frac{1}{r_i - s_k} \right] \left[ \frac{\kappa_1 + 1}{8} + \frac{\mu_0(\kappa_2 + 1)}{8\mu_2} \right] \right\} \right] = \frac{1}{h} M(s) \quad (15)$$

$$\frac{b}{2(a_2 - a_1)} \sum W_i(r_i) g(r_i) = 1 \quad (16)$$

where  $r_{1i}$  and  $s_{1k}$  are the roots of the related Jacobi polynomials and  $W_{1i}^N$  is the weighting constant

$$r_i = \cos\left(\frac{i\pi}{N+1}\right) \quad (i = 1, \dots, N) \quad (17)$$

$$s_k = \cos\left(\frac{\pi(2k-1)}{2(N+1)}\right) \quad (k = 1, \dots, N+1)$$

$$W_i^N = \pi \left( \frac{1 - r_i^2}{N+1} \right) \quad (i = 1, \dots, N)$$

The extra equation in (15) corresponds to the consistency condition of the original integral Equation (12). It may also be shown that the  $(N/2 + 1)$ -th equation in (15) is automatically satisfied. Thus, Equations (15) and (16) give  $2N + 2$  algebraic equations to determine the  $2N + 2$  unknowns  $G_i(r_{1i})$  and  $b$ . The system of equations is linear  $G_i(r_{1i})$  but highly nonlinear in  $b$ . Therefore, an interpolation and iteration scheme must be used to obtain this unknown.

### 3 | NUMERICAL APPROACH (FINITE ELEMENT METHOD)

This application, which includes a contact problem consisting of functionally graded material, has been analyzed through the finite element model. The problem handled in the analysis phase was modeled using the ANSYS Mechanical APDL 2013 package program, and finite element analysis was provided with the program's help [54].

Recent developments in computer technology have made FEM-based package programs more common and applicable in terms of analysis and design applications in engineering. As a result of this widespread use, the finite element method has become one of the most widely used methods for solving complex contact problems in the field of contact mechanics. Even for problems that seem impossible, a solution can be reached using the finite element method. Finite element analysis is done on the mesh system obtained by dividing the system into finite elements. At this stage, as the finite element dimensions get smaller, the shape is divided into more finite elements, and margin of error decreases. In

addition, it provides ease of application in systems with different and complex material properties without simplifying geometry. Dividing the shape into more finite elements by reducing the finite element size may increase the solution time of the system while also requiring computers with more sensitive technology. One of the most important reasons why the finite element method is widely preferred is these advantages [55–57].

The receding contact problem is modeled in two dimensions for our functionally graded layer to elastic and isotropic. The system is physically symmetrical in terms of geometry, material properties, and loading. Therefore, half of the problem is modeled. The material properties were determined for the contact problem modeled in two dimensions, and then the mesh system was created. Boundary conditions of the contact state and load steps are applied. Finally, solution options were determined, and analysis results were obtained.

In the analyses, geometric properties are taken as  $L = 100 \text{ m}$  (length of the layer in the  $x$  direction),  $h = 1 \text{ m}$  (thickness of the lower layer in the  $y$  direction), the load  $p_0 = 1000 \text{ N/m}$ , and the Poisson's ratio is given as constant for layer  $\nu = 0.25$ . A code has been developed by changing the layers along the  $y$ -axis to define the material properties in functional grades in the ANSYS program and added to the program's log files. Other solution parameters vary according to the desired results and are selected accordingly.

In this method, a mesh structure is created that is divided into many interconnected small sub-regions of the structure to be solved. Each small subregion in this mesh structure is a finite element, and nodes connect each finite element. This mesh state of the structure divided into elements is also called the numerical model. In summary, this method is a mathematical expression of a physical system. In determining the appropriate element size, choosing the most ideal element size that can be applied for more precise calculations and to obtain more approximate results is very important. Because, as the selected element size decreases, that is, as the number of finite elements in the mesh structure increases, more convergent results are obtained. The first dimension selected in the application was reduced to the ideal size that would not affect the analysis results significantly, and the mesh structure was created using the ideal size obtained. As a result, the mesh structure we created under the appropriate boundary conditions using the selected element dimensions contains 25,369 elements and 44,944 node points. We have determined that the building element we will use in the application is the PLANE183 element defined in the ANSYS program. The PLANE183 element is a non-rotational element with eight nodes and two degrees of freedom for each node. In addition, this structural element can be displaced and deformed in the  $x$  and  $y$  directions. It provides good performance compared to other elements due to its four nodal points in forming the mesh structure and is resistant to large-scale deformations. Modeling the existing contact problem in our study is another important issue. For this, contact pair TARGE169 and CONTA172 elements, which are quite compatible with each other, were selected. The harmony between these two elements can be expressed as TARGE169 element displacement, applied loads and moments are in harmony with each other in defining the CONTA172 sliding contact state. A total of 2097 lines of contact elements and 4194 contact nodes exist in the finite element model. Finally, the mesh structure, contact elements, and boundary conditions of the application are given in Figure 2. The deformed shape that occurs after the analysis of these models is shown in Figure 3.

## 4 | NUMERICAL EXAMPLE AND RESULT DISCUSSION

In this part, the contact areas and contact stresses that become under various loads, materials, and geometric properties are examined using ET and FEM. The results obtained from the numerical solutions are presented with figures and evaluated. In all solutions, the values of  $\mu_0/\mu_2 = 1$  and  $\kappa_1/\kappa_2 = 1$  were used. Other values related to material, loading, and geometry are considered depending on the ratios used in the analyses. The start distance of the distributed load ( $a_1$ ) and the end distance of the distributed load ( $a_2$ ) values change in the change of rates. At ( $a_1/h$ ) and ( $a_2/h$ ) ratios,  $h$  is kept constant. The dimensionless parameters are given below.

$a_1/h$ : The start distance of the distributed load.

$a_2/h$ : The end distance of the distributed load.

$\beta$ : The non-homogeneity parameter of the FG layer.

The output parameter:

$p_1(x)/p_0$ : The contact stresses between the HP and the FG layer.

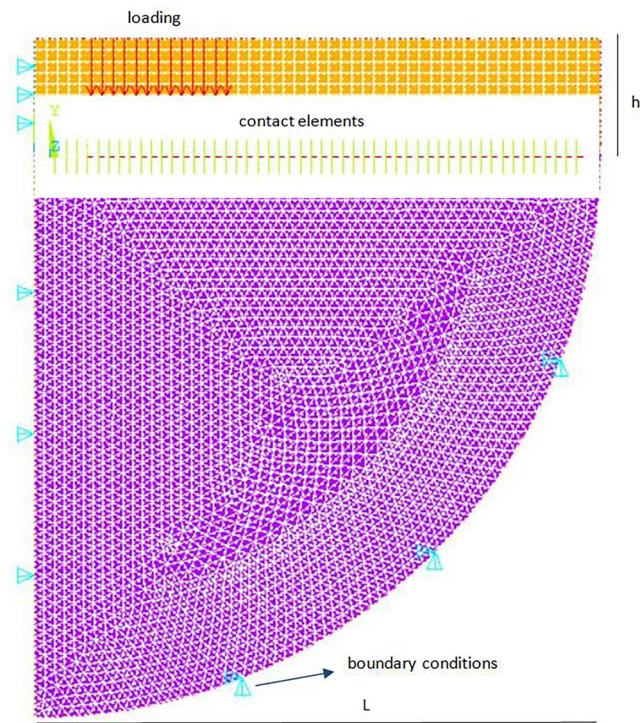


FIGURE 2 Mesh structure of the geometry. [Colour figure can be viewed at [wileyonlinelibrary.com](https://onlinelibrary.wiley.com/doi/10.1002/nme.11069)]

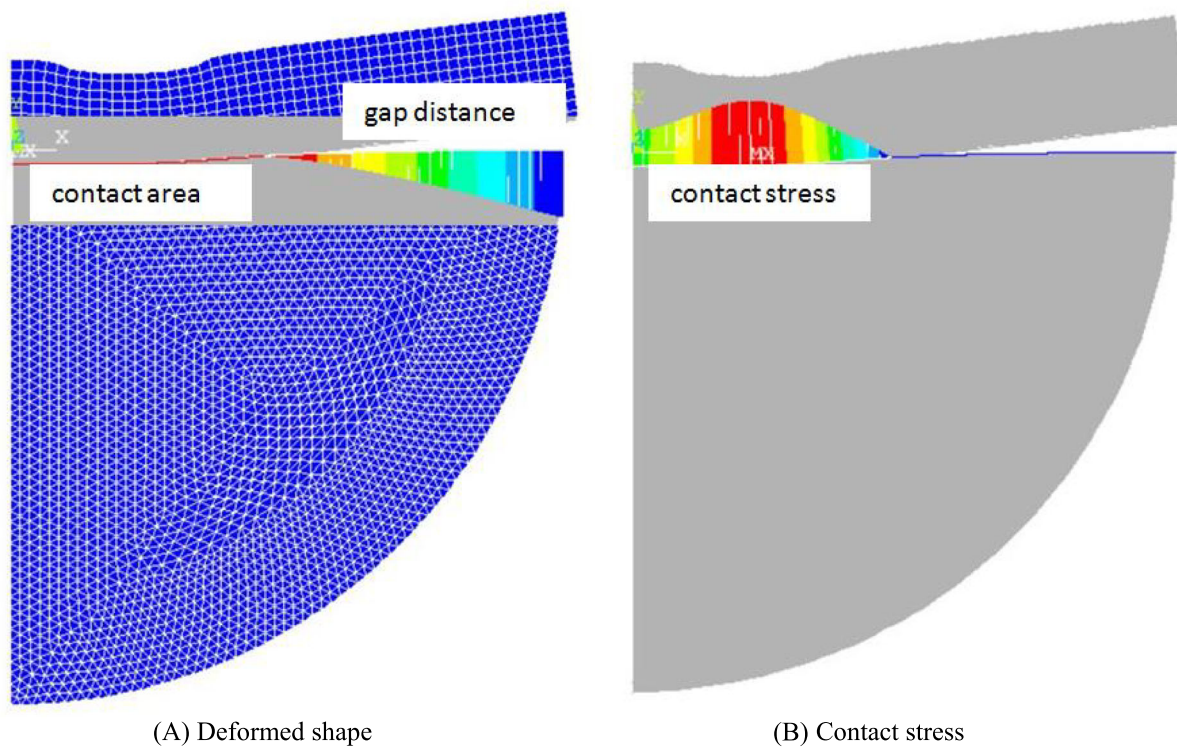


FIGURE 3 Deformed geometry of the finite element model. [Colour figure can be viewed at [wileyonlinelibrary.com](https://onlinelibrary.wiley.com/doi/10.1002/nme.11069)]



$b/h$ : The contact areas between the HP and the FG layer.

The harmony of the results was evaluated by considering the mean absolute error ( $E$ ). Mean absolute percent error is employed as the conformity function to evaluate the performance of the numerical results and is defined as [58].

$$\%E = \left| \frac{R_{ETi} - R_{FEMi}}{R_{ETi}} \right| \times 100 \quad (i = 1, 2, 3, \dots, n) \quad (18)$$

where  $R_{ETi}$  and  $R_{FEMi}$  are the analytical and numerical results of contact areas and contact stresses.  $n$  denotes the total number of results.

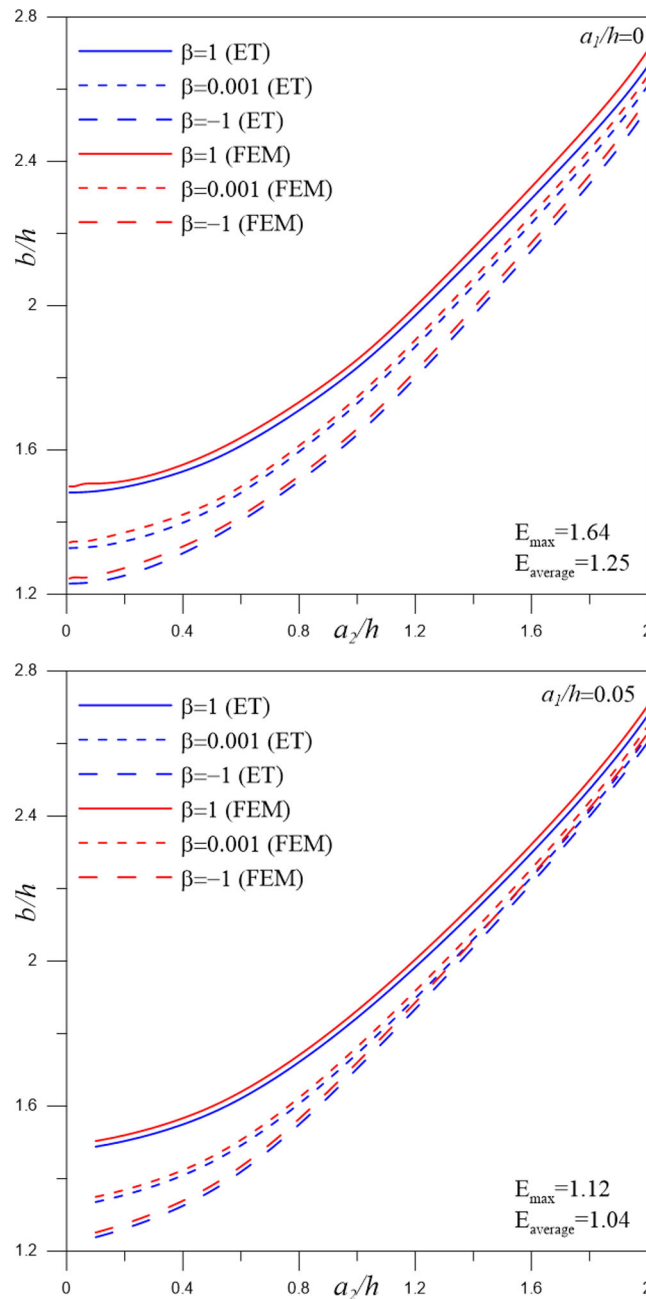


FIGURE 4 Change of contact area ( $b/h$ ) with ( $a_2/h$ ). [Colour figure can be viewed at [wileyonlinelibrary.com](http://wileyonlinelibrary.com)]

## 4.1 | Contact area

In Figure 4, the start distance of the distributed load is kept constant ( $a_1/h = 0$  and  $a_1/h = 0.05$ ). The contact areas ( $b/h$ ) change is shown for the different non-homogeneity parameter ( $\beta = 1$ ,  $\beta = 0.001$ , and  $\beta = -1$ ) values selected according to the end distance of the distributed load ( $a_2/h$ ). Accordingly, it is observed that the contact areas ( $b/h$ ) increase with increasing the end distance of the distributed load ( $a_2/h$ ). In Figure 5, the end distance of the distributed load is kept constant ( $a_2/h = 1$ ). The contact areas ( $b/h$ ) change is shown for the different non-homogeneity parameter ( $\beta$ ) values selected according to the start distance of the distributed load ( $a_1/h$ ). Accordingly, it is observed that the contact areas ( $b/h$ ) increase with the increasing start distance of the distributed load ( $a_1/h$ ). In addition, it is observed in Figures 4 and 5 that as the value of the non-homogeneity parameter ( $\beta$ ) increases, the contact areas ( $b/h$ ) also increase.

## 4.2 | Contact stress

The contact stresses between the FG layer and the HP reach the maximum value at the axis of symmetry ( $x = 0$ ), while the value is zero at the endpoints of contact ( $x = \pm b$ ). At ( $a_1/h$ ) and ( $a_2/h$ ) ratios,  $h$  is kept constant. The start distance of the distributed load ( $a_1$ ) and the end distance of the distributed load ( $a_2$ ) values change in the change of rates. In Figures (6–9), the contact stress variations are shown for different values of the end distance of the distributed load ( $a_2/h$ ), the start distance of the distributed load ( $a_1/h$ ), and the non-homogeneity parameter ( $\beta$ ). As can be seen from Figures 6 and 7, the non-homogeneity parameter ( $\beta$ ) increases, and the contact stresses ( $p_1(x)/p_0$ ) decrease in the regions close to the symmetry axis and increase as they approach the point where the contact ends. As the end distance of the distributed load ( $a_2/h$ ) increases, the contact stresses ( $p_1(x)/p_0$ ) increase (Figure 8). It can be seen from Figure 9 that as the start distance of the distributed load ( $a_1/h$ ) increases, the contact stresses ( $p_1(x)/p_0$ ) decrease.

Table 1 presents the similarity of results of FEM and ET methods for contact stress and contact area shown in Figures 6–9 using root-mean-square error (RMSE) and coefficient of determination ( $R^2$ ). The harmony of results with each other was assessed by calculating RMSE and  $R^2$ . It is found that non-dimensional contact stress and contact area acquired from FEM and ET agree well.

A nominal acquired RMSE amount demonstrates that the methods are harmonious. The near this value is to zero, the near the two solutions are to each other.  $R^2$  is a statistical statement that numerically indicates the correlation between FEM and ET results. This value ranges from 0 to 1 and  $R^2 > 0.80$  indicates a high correlation between FEM and ANN results. The RMSE and  $R^2$  can be expressed as follows [38].

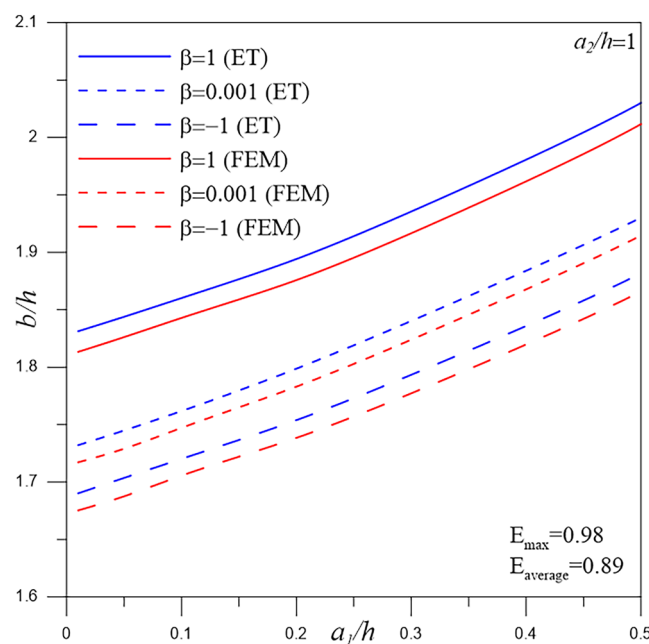


FIGURE 5 Change of contact area ( $b/h$ ) with ( $a_1/h$ ). [Colour figure can be viewed at [wileyonlinelibrary.com](http://wileyonlinelibrary.com)]

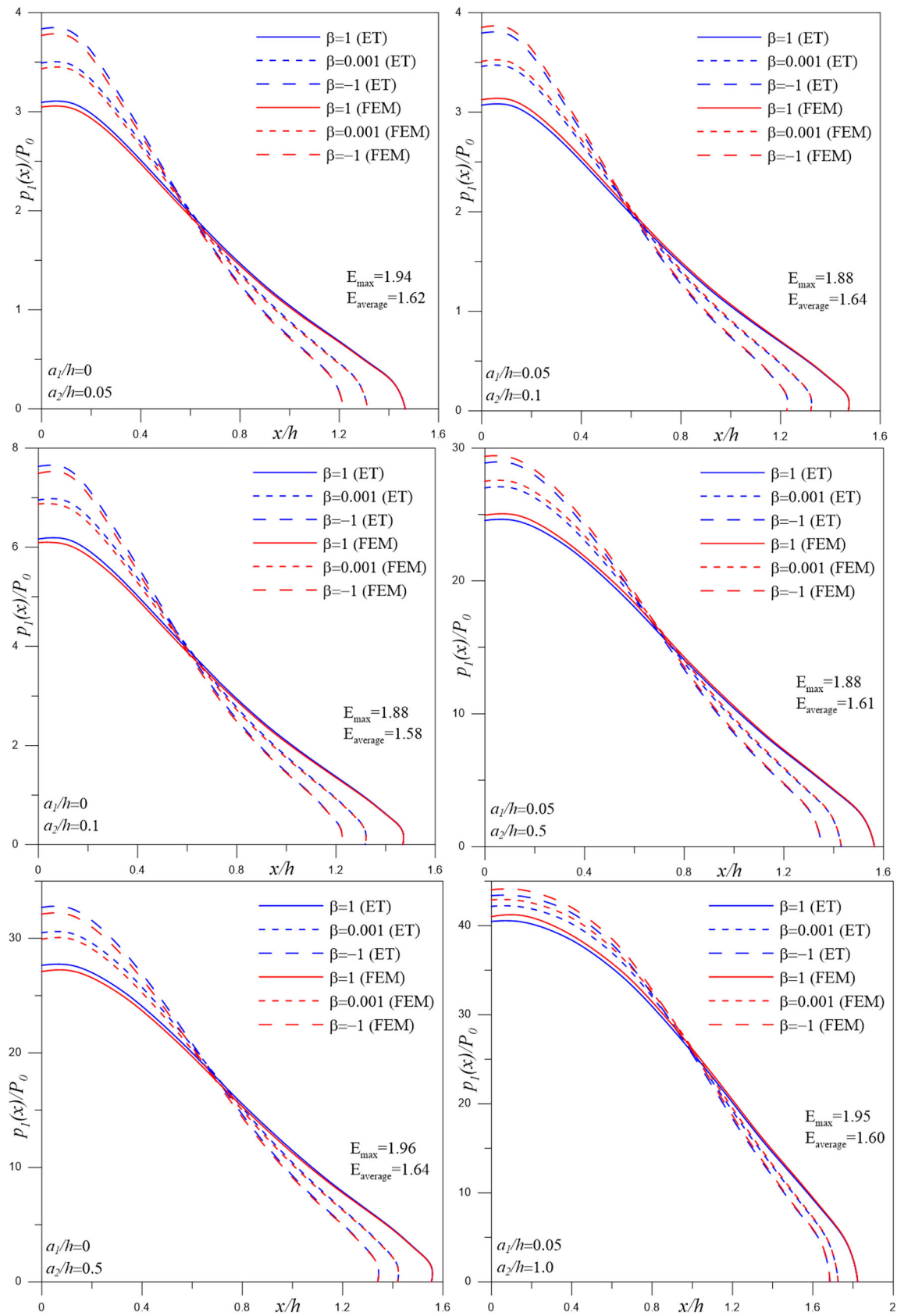


FIGURE 6 Change of contact stress ( $p_1(x)/p_0$ ) with ( $\beta$ ) for ( $a_2/h$ ). [Colour figure can be viewed at [wileyonlinelibrary.com](http://wileyonlinelibrary.com)]

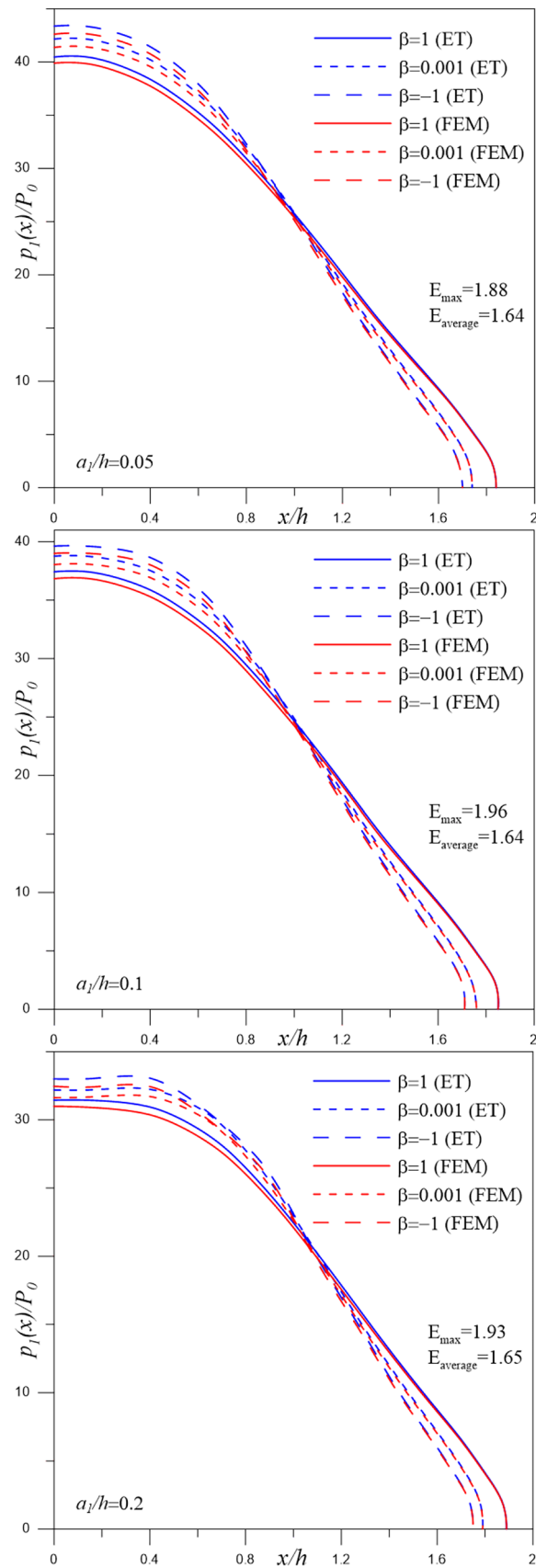


FIGURE 7 Change of contact stress ( $p_1(x)/p_0$ ) with ( $\beta$ ) for ( $a_1/h$ ), ( $a_2/h = 1$ ). [Colour figure can be viewed at [wileyonlinelibrary.com](http://wileyonlinelibrary.com)]

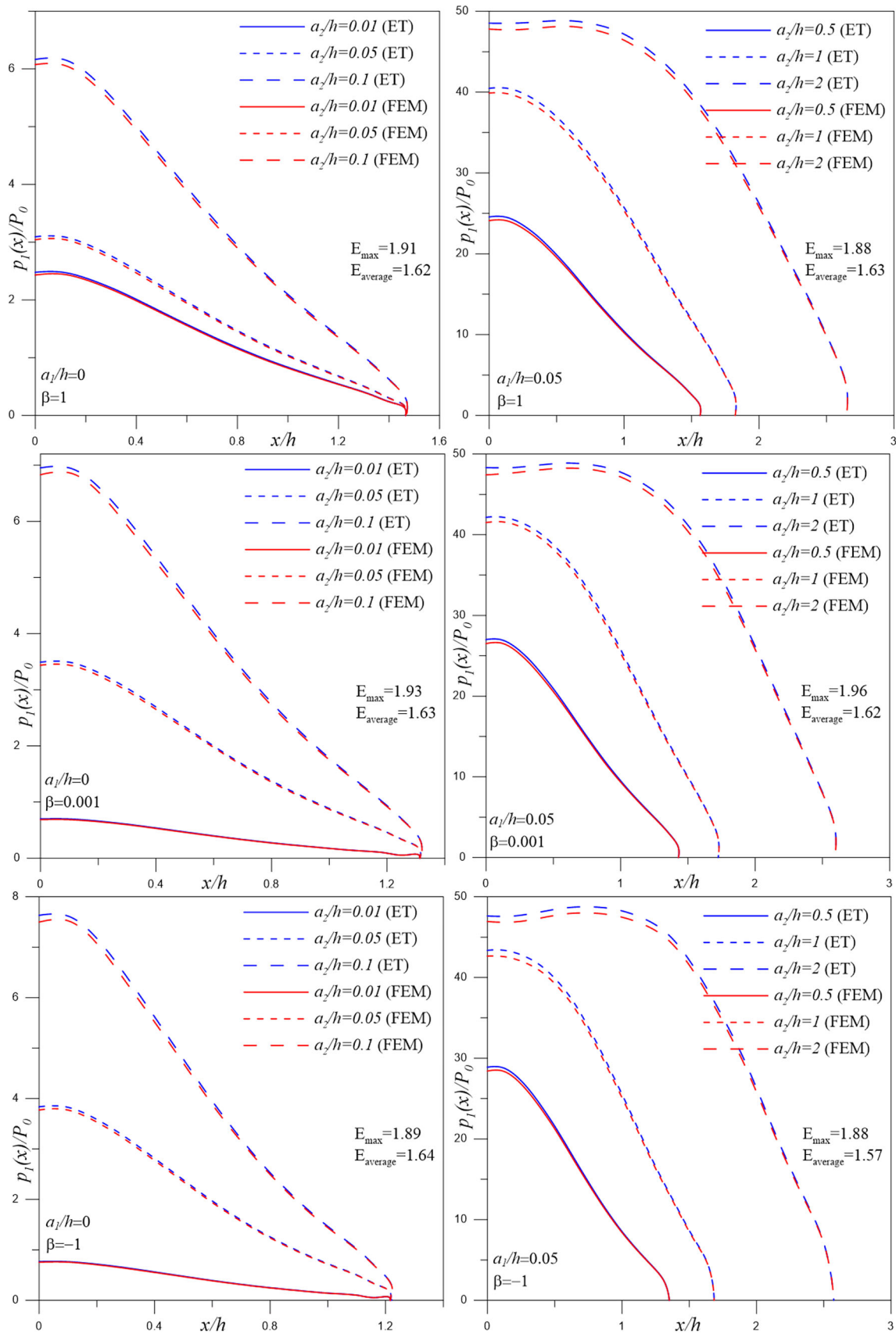


FIGURE 8 Change of contact stress ( $p_1(x)/p_0$ ) with ( $a_2/h$ ) for ( $\beta$ ). [Colour figure can be viewed at [wileyonlinelibrary.com](http://wileyonlinelibrary.com)]

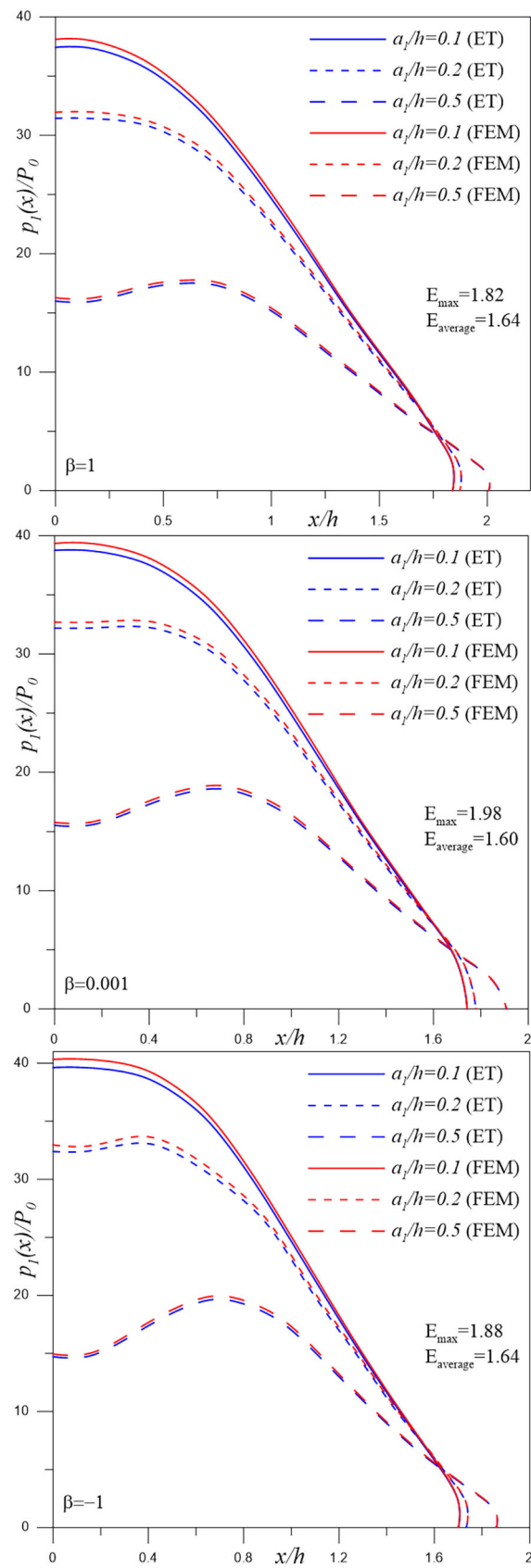
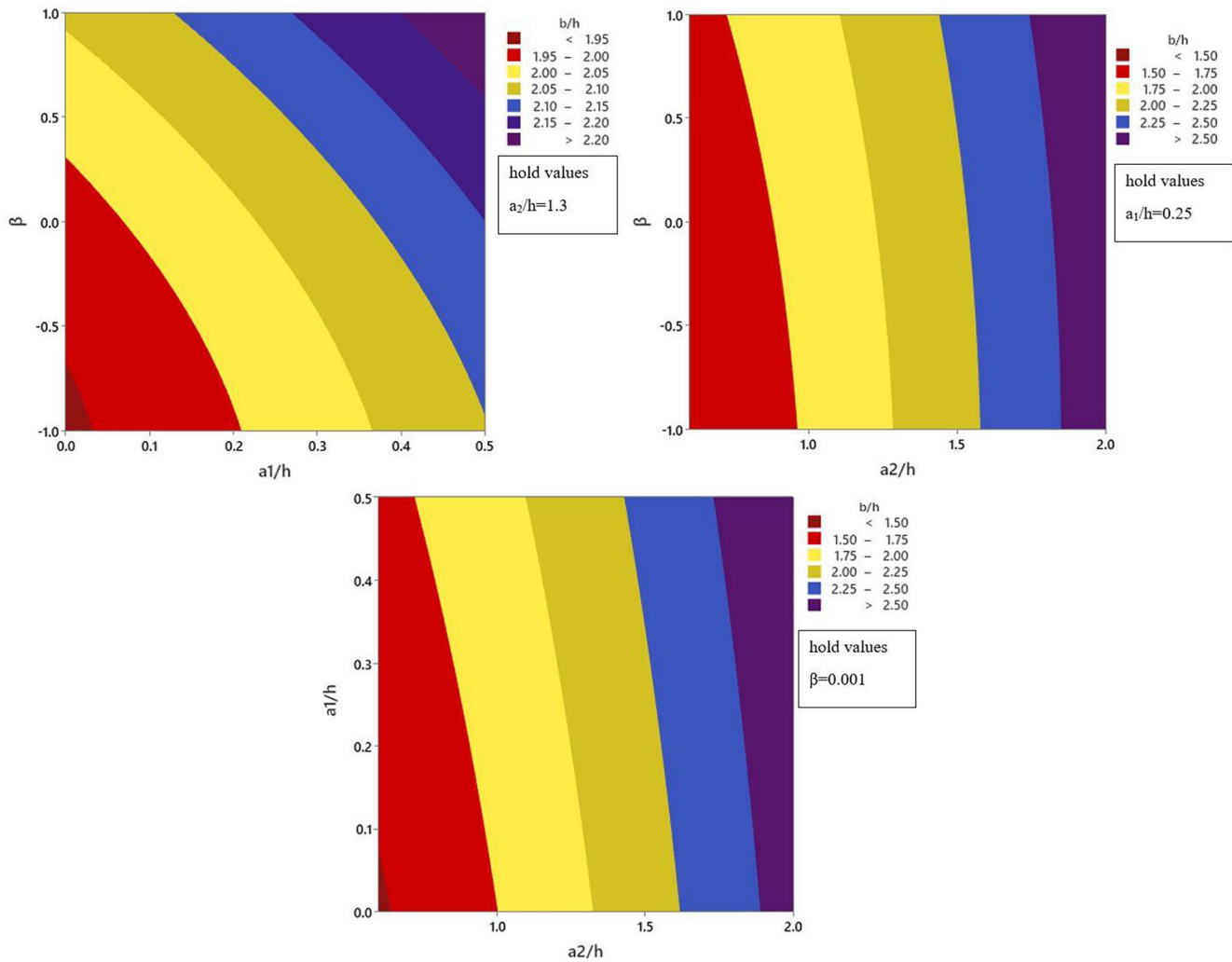


FIGURE 9 Change of contact stress ( $p_f(x)/p_0$ ) with ( $a_1/h$ ) for ( $\beta$ ), ( $a_2/h = 1$ ). [Colour figure can be viewed at [wileyonlinelibrary.com](http://wileyonlinelibrary.com)]

TABLE 1 RMSE and  $R^2$  for contact area and contact stress.

Figures	RMSE	$R^2$
Figure 6	0.0106	0.99998
Figure 7	0.0126	0.99997
Figure 8	0.0149	0.99979
Figure 9	0.0135	0.99984

FIGURE 10 The contour plot contact area ( $b/h$ ). [Colour figure can be viewed at [wileyonlinelibrary.com](http://wileyonlinelibrary.com)]

$$RMSE = \sqrt{\frac{1}{n} \sum_i^n (R_{FEM_i} - R_{ANN_i})^2}, \quad (i = 1, 2, 3, \dots, n) \quad (19)$$

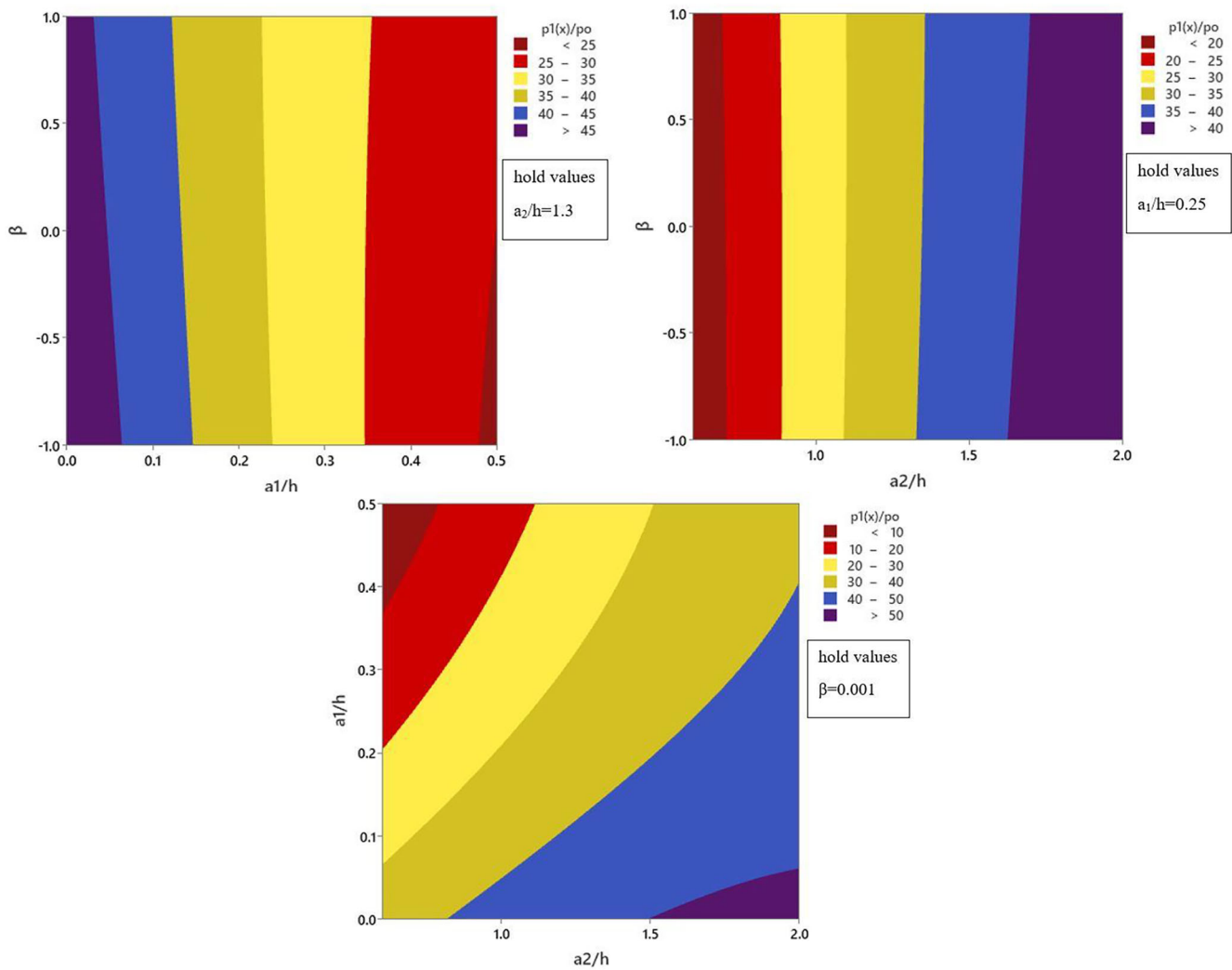


FIGURE 11 The contour plot contact stress ( $p_1(x)/p_0$ ). [Colour figure can be viewed at [wileyonlinelibrary.com](https://onlinelibrary.wiley.com/doi/10.1002/mm.10129)]

$$R^2 = 1 - \frac{\sum_i^n (R_{FEM_i} - R_{ANN_i})^2}{\sum_i^n (R_{FEM_i} - \bar{R}_{FEM})^2}, \quad (i = 1, 2, 3, \dots, n) \quad (20)$$

### 4.3 | Statistical analysis

To determine the statistical significance of the model, the results from the theoretical solution were analyzed using analysis of variance (ANOVA). The effect of independent variables (the start distance of the distributed load, the end distance of the distributed load, and the non-homogeneity parameter of the FG layer) on the contact stresses and areas between the HP and the FG layer were evaluated with contour plots by MINITAB 19 software (Figures 10 and 11). In the figures, a value was taken as a constant, and the relationship between the other two variables was discussed. The contact area increases when any two variables increase, and one variable is kept constant (Figure 10). On the other hand, the contact stress decreases when  $a_1/h$  and  $\beta$  increase and increases when  $a_2/h$  increases (Figure 11). When the figures are considered, the results are most affected by  $a_2/h$  and then  $a_1/h$  and  $\beta$ , respectively.



## 5 | CONCLUSIONS

Contact mechanics is a significant field in the solution of engineering problems. Two important parameters of contact mechanics are contact area and contact stress. Obtaining these two values will facilitate the solution of engineering problems. Several methods can be used to find these values. However, researchers need to find the most useful and correct way.

This paper presents the contact analysis between the functionally graded layer and the elastic half-plane. For this purpose, different analyses are actualized with analytical and numerical methods. The analytical method based on the theory of elasticity in contact problems gives exact results. The contact area and contact stress results were obtained by a numerical method using the FEM, and their accuracy was examined.

Then, the problem was handled based on the ET and FEM used for different problem parameters. The following results were obtained based on the findings of the study.

- When the value of a non-homogeneity parameter is increased, the contact stress decreases, and the contact area increases.
- When the variation of the starting and ending distances of the distributed load increases the width of the distributed load, the contact area and maximum contact stress increase.
- The distributed load width and non-homogeneity parameter significantly affect the results. However, the distributed load width is more effective.
- The results obtained from the FEM and ET methods are in good agreement with each other. The error rates were found to be very low. Therefore, the FEM can be used in practical solutions to the contact problem.

### CONSENT TO PARTICIPATE

No external participants have contributed to the work discussed in this manuscript.

### CONSENT FOR PUBLICATION

The authors give their full consent to the editor to publish this article if accepted.

### AUTHOR CONTRIBUTIONS

**Murat Yaylacı:** Conceptualization; methodology; software; data curation; investigation; validation; formal analysis; supervision; visualization; project administration; resources; writing—original draft. **Müjgen Yaylı:** Investigation; resources; conceptualization; formal analysis; data curation. **Şevval Öztürk:** Writing—original draft; resources; data curation. **Sevil Ay:** Writing—original draft; data curation; resources. **Mehmet Emin Özdemir:** Software; formal analysis; data curation; methodology; validation. **Ecren Uzun Yaylacı:** Conceptualization; methodology; software; data curation; investigation; validation; formal analysis; supervision; visualization; project administration; resources; writing—original draft. **Ahmet Birinci:** Methodology; conceptualization; investigation; data curation; supervision.

### CONFLICT OF INTEREST STATEMENT

The authors declare no conflicts of interest.

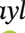
### ORCID

Murat Yaylacı  <https://orcid.org/0000-0003-0407-1685>

Şevval Öztürk  <https://orcid.org/0009-0002-1406-6302>

Sevil Ay  <https://orcid.org/0000-0003-3290-2343>

Mehmet Emin Özdemir  <https://orcid.org/0000-0001-7983-7265>

Ecren Uzun Yaylacı  <https://orcid.org/0000-0002-2558-2487>

Ahmet Birinci  <https://orcid.org/0000-0002-5913-7699>

### REFERENCES

1. H. Hertz, *Gesammelte Werke von Heinrich Hertz*, Leipzig, 1895.
2. M. Yaylacı, E. Uzun Yaylacı, M. E. Özdemir, S. Ay, and Ş. Öztürk, *Implementation of finite element and artificial neural network methods to analyze the contact problem of a functionally graded layer containing crack*, *Steel Compos. Struct.* **45** (2022), no. 4, 501–511, DOI [10.12989/scs.2022.45.4.501](https://doi.org/10.12989/scs.2022.45.4.501).

3. M. Yaylacı, M. Abanoz, E. Uzun Yaylacı, H. Ölmez, M. D. Sekban, and A. Birinci, *The contact problem of the functionally graded layer resting on rigid foundation pressed via rigid punch*, *Steel Compos. Struct.* **43** (2022), no. 5, 661–672, DOI [10.12989/scs.2022.43.5.661](https://doi.org/10.12989/scs.2022.43.5.661).
4. M. Yaylacı, B. Şengül Şabano, M. E. Özdemir, and A. Birinci, *Solving the contact problem of functionally graded layers resting on a homogeneous half-plane and pressed with a uniformly distributed load by analytical and numerical methods*, *Struct. Eng. Mech.* **82** (2022), no. 3, 401–416, DOI [10.12989/sem.2022.82.3.401](https://doi.org/10.12989/sem.2022.82.3.401).
5. M. Yaylacı, M. Abanoz, E. Uzun Yaylacı, H. Ölmez, M. D. Sekban, and A. Birinci, *Evaluation of the contact problem of functionally graded layer resting on rigid foundation pressed via rigid punch by analytical and numerical (FEM and MLP) methods*, *Arch. Appl. Mech.* **92** (2022), 1953–1971, DOI [10.1007/s00419-022-02159-5](https://doi.org/10.1007/s00419-022-02159-5).
6. A. Emamian, A. Amiri Delouei, S. Karimnejad, and D. Jing, *Analytical solution for temperature distribution in functionally graded cylindrical shells under convective cooling*, *Math. Methods. Appl. Sci.* **46** (2023), no. 10, 11442–11461, DOI [10.1002/mma.7819](https://doi.org/10.1002/mma.7819).
7. R. D. Nedin, A. O. Vatulyan, and I. V. Bogachev, *Direct and inverse problems for prestressed functionally graded plates in the framework of the Timoshenko model*, *Math. Methods. Appl. Sci.* **41** (2018), no. 4, 1600–1618, DOI [10.1002/mma.4688](https://doi.org/10.1002/mma.4688).
8. V. V. Dudarev, A. O. Vatulyan, R. M. Mnukhin, and R. D. Nedin, *Concerning an approach to identifying the Lamé parameters of an elastic functionally graded cylinder*, *Math. Methods. Appl. Sci.* **43** (2020), no. 11, 6861–6870, DOI [10.1002/mma.6428](https://doi.org/10.1002/mma.6428).
9. H. Benaissa, E. H. Benkhira, R. Fakhar, and A. Hachlaf, *Quasistatic frictional thermo piezoelectric contact problem*, *Math. Methods. Appl. Sci.* **42** (2019), no. 4, 1292–1311, DOI [10.1002/mma.5442](https://doi.org/10.1002/mma.5442).
10. N. Shavlakadze and T. Jamaspishvili, *The singular integro differential equations and its applications in the contact problems of elasticity theory*, *Math. Methods. Appl. Sci.* (2021), 1–12, DOI [10.1002/mma.7493](https://doi.org/10.1002/mma.7493).
11. G. Griso and J. Orlik, *Homogenization of contact problem with Coulomb's friction on periodic cracks*, *Math. Methods. Appl. Sci.* **42** (2019), no. 18, 6435–6458, DOI [10.1002/mma.5749](https://doi.org/10.1002/mma.5749).
12. I. Çömez, V. Kahya, and R. Erdöl, *Plane receding contact problem for a functionally graded layer supported by two quarter-planes*, *Arch. Mech.* **70** (2018), no. 6, 485–504, DOI [10.24423/aom.2846](https://doi.org/10.24423/aom.2846).
13. S. El-Borgi and I. Çömez, *A receding frictional contact problem between a graded layer and a homogeneous substrate pressed by a rigid punch*, *Mech. Mater.* **114** (2017), 201–214, DOI [10.1016/j.mechmat.2017.08.003](https://doi.org/10.1016/j.mechmat.2017.08.003).
14. S. El-Borgi, R. Abdelmoula, and L. Keer, *A receding contact plane problem between a functionally graded layer and a homogeneous substrate*, *Internat. J. Solids Structures.* **43** (2006), no. 3–4, 658–674, DOI [10.1016/j.ijsolstr.2005.04.017](https://doi.org/10.1016/j.ijsolstr.2005.04.017).
15. M. Rhimi, S. El-Borgi, W. Ben Saïd, and F. Ben Jemaa, *A receding contact axisymmetric problem between a functionally graded layer and a homogeneous substrate*, *Internat. J. Solids Structures.* **46** (2009), no. 20, 3633–3642, DOI [10.1016/j.ijsolstr.2009.06.008](https://doi.org/10.1016/j.ijsolstr.2009.06.008).
16. M. Rhimi, S. El-Borgi, and N. Lajnef, *A double receding contact axisymmetric problem between a functionally graded layer and a homogeneous substrate*, *Mech. Mater.* **43** (2011), no. 12, 787–798, DOI [10.1016/j.mechmat.2011.08.013](https://doi.org/10.1016/j.mechmat.2011.08.013).
17. N. I. Muskhelishvili, *Some basic problems of mathematical theory of elasticity*, Noordhoff, Groningen, The Netherlands, 1953.
18. A. H. England, *Complex variable methods in elasticity*, Wiley Interscience, London, 1971.
19. G. G. Adams, *An elastic strip pressed against an elastic half plane by a steadily moving force*, *J. Theoret. Appl. Mech.* **45** (1978), no. 1, 89–94, DOI [10.1115/1.3424279](https://doi.org/10.1115/1.3424279).
20. H. Saito and T. Terasawa, *Steady-state vibrations of a beam on a Pasternak foundation for moving loads*, *J. Theoret. Appl. Mech.* **47** (1980), no. 4, 879–883, DOI [10.1115/1.3153807](https://doi.org/10.1115/1.3153807).
21. J. P. Dempsey, Z. G. Zhao, L. Minnetyan, and H. Li, *Plane contact of an elastic layer supported by a Winkler foundation*, *J. Theoret. Appl. Mech.* **57** (1990), no. 1, 974–980, DOI [10.1115/1.2897670](https://doi.org/10.1115/1.2897670).
22. A. E. Giannakopoulos and S. Suresh, *Indentation of solids with gradients in elastic properties: part I. Point force and part II. Axisymmetric indentors*, *Internat. J. Solids Structures.* **34** (1997), no. 9, 2357–2428, DOI [10.1016/S0020-7683\(96\)00172-2](https://doi.org/10.1016/S0020-7683(96)00172-2).
23. C. Chao and B. Gao, *Rigid stamp indentation for thermoelastic half plane*, *Internat. J. Solids Structures.* **37** (2000), 4635–4654, DOI [10.1016/S0020-7683\(99\)00138-9](https://doi.org/10.1016/S0020-7683(99)00138-9).
24. M. A. Güler and F. Erdoğan, *Contact mechanics of graded coatings*, *Internat. J. Solids Structures.* **41** (2004), no. 14, 3865–3889, DOI [10.1016/j.ijsolstr.2004.02.025](https://doi.org/10.1016/j.ijsolstr.2004.02.025).
25. L. L. Ke and Y. S. Wang, *Two-dimensional contact mechanics of functionally graded materials with arbitrary spatial variations of material properties*, *Internat. J. Solids Structures.* **43** (2006), no. 18–19, 5779–5798, DOI [10.1016/j.ijsolstr.2005.06.081](https://doi.org/10.1016/j.ijsolstr.2005.06.081).
26. J. Yang and L. L. Ke, *Two-dimensional contact problem for a coating-graded layer- substrate structure under a rigid cylindrical punch*, *Int. J. Mech. Sci.* **50** (2008), no. 6, 985–994, DOI [10.1016/j.ijmecsci.2008.03.002](https://doi.org/10.1016/j.ijmecsci.2008.03.002).
27. S. M. Aizikovich, A. S. Vasil'ev, L. I. Krenev, I. S. Trubchik, and N. M. Seleznev, *Contact problems for functionally graded materials of complicated structure*, *Mech. Compos. Mater.* **47** (2011), 539–548, DOI [10.1007/s11029-011-9232-8](https://doi.org/10.1007/s11029-011-9232-8).
28. S. Volkov, S. Aizikovich, Y. S. Wang, and I. Fedotov, *Analytical solution of axisymmetric contact problem about indentation of a circular indenter into a soft functionally graded elastic layer*, *Acta. Mech. Sin.* **29** (2013), no. 2, 196–201, DOI [10.1007/s10409-013-0022-5](https://doi.org/10.1007/s10409-013-0022-5).
29. J. Yan and X. Li, *Double receding contact plane problem between a functionally graded layer and an elastic layer*, *Eur. J. Mech. a Solids.* **53** (2015), 143–150, DOI [10.1016/j.euromechsol.2015.04.001](https://doi.org/10.1016/j.euromechsol.2015.04.001).
30. M. K. Singh, A. K. Rahul, S. Saha, S. Paul, R. Tiwari, and S. Nandi, *On generalized Rayleigh waves in a pre-stressed piezoelectric medium*, *Internat. J. Modern. Phys. C.* **35** (2024), no. 2, 2440006, DOI [10.1142/S0129183124400060](https://doi.org/10.1142/S0129183124400060).
31. M. K. Singh and P. Alam, *Surface wave analysis in orthotropic composite structure with irregular interfaces*, *Int. J. Appl. Comput. Math.* **6** (2020), 13, DOI [10.1007/s40819-019-0745-5](https://doi.org/10.1007/s40819-019-0745-5).

32. P. Alam, T. Nahid, B. Al Alwan, and A. Saha, *Rotating radial vibrations in human bones (femoral, mandibular and tibia) and crystals (mg, co, cd, Zn and beryl) made cylindrical shell under magnetic field and hydrostatic stress*, *Mech. Adv. Mater. Struct.* **30** (2023), no. 13, 2684–2700, DOI [10.1080/15376494.2022.2062499](https://doi.org/10.1080/15376494.2022.2062499).
33. J. S. Mario and P. Alam, *A multi-layered model of Newtonian viscous liquid, fiber-reinforced and poro-elastic media over a self-weighted half-space to investigate the SH-wave interactions*, *Mech. Adv. Mater. Struct.* (2023), 1–13, DOI [10.1080/15376494.2023.2256537](https://doi.org/10.1080/15376494.2023.2256537).
34. P. Alam, K. S. Singh, R. Ali, I. A. Badruddin, T. M. Yunus Khan, and S. Kamangar, *Dispersion and attenuation of SH-waves in a temperature-dependent Voigt-type viscoelastic strip over an inhomogeneous half-space*, *Z. Angew. Math. Mech.* **101** (2021), no. 12, e202000223, DOI [10.1002/zamm.202000223](https://doi.org/10.1002/zamm.202000223).
35. P. Alam, S. Jena, I. A. Badruddin, T. M. Y. Khan, and S. Kamangar, *Attenuation and dispersion phenomena of shear waves in anelastic and elastic porous strips*, *Eng. Comput.* **38** (2021), no. 7, 3132–3149, DOI [10.1108/EC-07-2020-0381](https://doi.org/10.1108/EC-07-2020-0381).
36. S. Chowdhury, S. Kundu, P. Alam, and S. Gupta, *Dispersion of Stoneley waves through the irregular common interface of two hydrostatic stressed MTI media*, *Sci. Iran.* **28** (2021), no. 2, 837, 0–846, DOI [10.24200/sci.2020.52653.2820](https://doi.org/10.24200/sci.2020.52653.2820).
37. M. E. Özdemir and M. Yaylacı, *Research of the impact of material and flow properties on fluid-structure interaction in cage systems*, *Wind Struct.* **36** (2022), no. 1, 31–40.
38. M. Turan, E. Uzun Yaylacı, and M. Yaylacı, *Free vibration and buckling of functionally graded porous beams using analytical, finite element, and artificial neural network methods*, *Arch. Appl. Mech.* **93** (2022), 1351–1372, DOI [10.1007/s00419-022-02332-w](https://doi.org/10.1007/s00419-022-02332-w).
39. Y. Güvercin, M. Yaylacı, A. Dizdar, A. Kanat, E. Uzun Yaylacı, S. Ay, A. A. Abdioglu, and A. Şen, *Biomechanical analysis of odontoid and transverse atlantal ligament in humans with ponticulus posticus variation under different loading conditions: finite element study*, *Injury.* **53** (2022), 3879–3886, DOI [10.1016/j.injury.2022.10.003](https://doi.org/10.1016/j.injury.2022.10.003).
40. Y. Güvercin, A. A. Abdioglu, A. Dizdar, E. Uzun Yaylacı, and M. Yaylacı, *Suture button fixation method used in the treatment of syndesmosis injury: a biomechanical analysis of the effect of the placement of the button on the distal tibiofibular joint in the mid-stance phase with finite elements method*, *Injury.* **53** (2022), 2437–2445, DOI [10.1016/j.injury.2022.05.037](https://doi.org/10.1016/j.injury.2022.05.037).
41. H. M. Numanoğlu, H. Ersoy, B. Akgöz, and Ö. Civalek, *A new eigenvalue problem solver for thermo-mechanical vibration of Timoshenko nanobeams by an innovative nonlocal finite element method*, *Math. Methods Appl. Sci.* **45** (2022), no. 5, 2592–2614, DOI [10.1002/mma.7942](https://doi.org/10.1002/mma.7942).
42. K. Kamila, K. Eva, and H. Slavka, *Pressure and stress analysis of liquid-filled cylindrical tank*, *Math. Methods Appl. Sci.* **45** (2022), no. 15, 8819–8834, DOI [10.1002/mma.7711](https://doi.org/10.1002/mma.7711).
43. M. A. Boukrra, S. Amdouni, and F. Delvare, *Fading regularization FEM algorithms for the Cauchy problem associated with the two dimensional biharmonic equation*, *Math. Methods Appl. Sci.* **46** (2023), no. 2, 2389–2412, DOI [10.1002/mma.8651](https://doi.org/10.1002/mma.8651).
44. K. B. Yilmaz, I. Çömez, B. Yildirim, M. A. Güler, and S. El-Borgi, *Frictional receding contact problem for a graded bilayer system indented by a rigid punch*, *Int. J. Mech. Sci.* **141** (2018), 127–142, DOI [10.1016/j.ijmecsci.2018.03.041](https://doi.org/10.1016/j.ijmecsci.2018.03.041).
45. I. Çömez, S. El-Borgi, and B. Yildirim, *Frictional receding contact problem of a functionally graded layer resting on a homogeneous coated half-plane*, *Arch. Appl. Mech.* **90** (2020), 2113–2131, DOI [10.1007/s00419-020-01712-4](https://doi.org/10.1007/s00419-020-01712-4).
46. R. Cao and C. Mi, *On the receding contact between a graded and a homogeneous layer due to a flat-ended indenter*, *Math. Mech. Solids.* **27** (2022), no. 5, 775–793, DOI [10.1177/10812865211043152](https://doi.org/10.1177/10812865211043152).
47. N. Schwarzer, H. Djabella, F. Richter, and R. D. Arnell, *Comparison between analytical and FEM calculations for the contact problem of spherical indenters on layered materials*, *Thin Solid Films.* **270** (1995), no. 1–2, 279–282, DOI [10.1016/0040-6090\(95\)06922-4](https://doi.org/10.1016/0040-6090(95)06922-4).
48. M. A. Güler, Y. Alinia, and S. Adibnazari, *On the rolling contact problem of two elastic solids with graded coatings*, *Int. J. Mech. Sci.* **64** (2012), no. 1, 62–81, DOI [10.1016/j.ijmecsci.2012.08.001](https://doi.org/10.1016/j.ijmecsci.2012.08.001).
49. M. N. Abhilash and H. Murthy, *Finite element analysis of 2-d elastic contacts involving FGMs*, *Int. J. Comput. Methods Eng.* **15** (2014), no. 3, 253–257, DOI [10.1080/15502287.2014.882445](https://doi.org/10.1080/15502287.2014.882445).
50. Z. X. Liu, J. Yan, and C. W. Mi, *On the receding contact between a two-layer inhomogeneous laminate and a half-plane*, *Struct. Eng. Mech.* **66** (2018), no. 3, 329–341, DOI [10.12989/sem.2018.66.3.329](https://doi.org/10.12989/sem.2018.66.3.329).
51. F. Erdogan, G. D. Gupta, and T. S. Cook, *Numerical solution of singular integral equations, in methods of analysis and solution of crack problems*, Noordhoff, Groningen, 1973.
52. S. Krenk, *On quadrate formulas for singular integral-equations of 1st and 2nd kind*, *Quart. Appl. Math.* **33** (1975), no. 3, 225–232.
53. F. Erdoğan and G. D. Gupta, *On the numerical solution of singular integral equations*, *Quart. Appl. Math.* **29** (1972), 525–534.
54. ANSYS, *Mechanical APDL, ANSYS Contact Technology Guide*, Ansys, Inc., Canonsburg, Pennsylvania, U.S.A, 2013.
55. T. Y. Zhao, Y. X. Wang, and L. Chen, *Mathematical modeling and vibration analysis of rotating functionally graded porous spacecraft systems reinforced by graphene nanoplatelets*, *Math. Methods Appl. Sci.* (2022), 1–25, DOI [10.1002/mma.9189](https://doi.org/10.1002/mma.9189).
56. J. Flores, E. Salete, J. J. Benito, A. M. Vargas, and E. R. Conde, *Generalized finite difference method applied to solve seismic wave propagation problems. Examples of 3D simulations*, *Math. Methods Appl. Sci.* (2023), 1–21, DOI [10.1002/mma.9286](https://doi.org/10.1002/mma.9286).
57. I. Kološ, V. Michalcová, and L. Lausová, *Numerical modeling of the pressure coefficient of the circular cylinder*, *Math. Methods Appl. Sci.* **43** (2020), no. 13, 7579–7594, DOI [10.1002/mma.5901](https://doi.org/10.1002/mma.5901).
58. A. R. Hadhoud, A. A. Rageh, and P. Agarwal, *Numerical method for solving two dimensional of the space and space-time fractional coupled reaction diffusion equations*, *Math. Methods Appl. Sci.* **46** (2023), no. 5, 6054–6076, DOI [10.1002/mma.8891](https://doi.org/10.1002/mma.8891).

**How to cite this article:** M. Yaylacı, M. Yaylı, Ş. Öztürk, S. Ay, M. E. Özdemir, E. U. Yaylacı, and A. Birinci, *Examining the contact problem of a functionally graded layer supported by an elastic half-plane with the analytical and numerical methods*, *Math. Meth. Appl. Sci.* (2024), 1–21. DOI [10.1002/mma.10129](https://doi.org/10.1002/mma.10129).

## APPENDIX A: COEFFICIENTS

$$A_1 = \left( \bar{p} (e^{hn_2} (C_4 D_2 D_3 - C_3 D_2 D_4) + e^{hn_3} (C_2 D_3 D_4 + C_4 D_2 D_3) + e^{hn_4} (C_3 D_2 D_4 + C_2 D_3 D_4)) \right. \\ \left. + F (e^{h(n_2+n_3)} (C_3 D_2 D_4 - C_2 D_3 D_4) + e^{h(n_2+n_4)} (C_2 D_3 D_4 - C_4 D_2 D_3) + e^{h(n_3+n_4)} (C_4 D_2 D_3 - C_3 D_2 D_4)) \right) / \Delta \quad (A1)$$

$$A_2 = \left( \bar{p} (e^{hn_1} (C_3 D_1 D_4 - C_4 D_1 D_3) + e^{hn_3} (C_4 D_1 D_3 - C_1 D_3 D_4) + e^{hn_4} (C_1 D_3 D_4 - C_3 D_1 D_4)) \right. \\ \left. + F (e^{h(n_1+n_3)} (-C_3 D_1 D_4 + C_1 D_3 D_4) + e^{h(n_1+n_4)} (-C_1 D_3 D_4 + C_4 D_1 D_3) + e^{h(n_3+n_4)} (-C_4 D_1 D_3 + C_3 D_1 D_4)) \right) / \Delta \quad (A2)$$

$$A_3 = \left( \bar{p} (e^{hn_1} (-C_2 D_1 D_4 + C_4 D_1 D_2) + e^{hn_2} (C_1 D_2 D_4 - C_4 D_1 D_2) + e^{hn_4} (C_2 D_1 D_4 - C_1 D_2 D_4)) \right. \\ \left. + F (e^{h(n_1+n_2)} (-C_1 D_2 D_4 + C_2 D_1 D_4) + e^{h(n_1+n_4)} (C_1 D_2 D_4 - C_4 D_1 D_2) + e^{h(n_2+n_4)} (-C_2 D_1 D_4 + C_4 D_1 D_4)) \right) / \Delta \quad (A3)$$

$$A_4 = \left( \bar{p} (e^{hn_1} (C_2 D_1 D_3 - C_3 D_1 D_2) + e^{hn_2} (-C_1 D_2 D_3 + C_3 D_1 D_2) + e^{hn_3} (C_1 D_2 D_3 - C_2 D_1 D_3)) \right. \\ \left. + F (e^{h(n_1+n_2)} (C_1 D_2 D_3 - C_2 D_1 D_4) + e^{h(n_1+n_3)} (-C_1 D_2 D_3 + C_3 D_1 D_2) + e^{h(n_2+n_3)} (C_2 D_1 D_3 - C_3 D_1 D_2)) \right) / \Delta \quad (A4)$$

$$B_1 = -P_2(\xi) \frac{(\kappa_2 - 1)}{2\xi} \quad (A5)$$

$$B_2 = -P_2(\xi) \quad (A6)$$

## APPENDIX B: $M(x)$ , $k(x,t)$ , AND $\Delta$

$$M(x) = \int_0^\infty \frac{-\xi(\kappa_1 - 1)}{\Delta \mu_0 e^{\beta h}} \{ (e^{nh_1} ((C_3 D_1 D_4 - C_4 D_1 D_3) M_2 + (C_4 D_1 D_2 - C_2 D_1 D_4) M_3 + (C_2 D_1 D_3 - C_3 D_1 D_2) M_4) \\ + (e^{nh_2} ((C_4 D_2 D_3 - C_3 D_2 D_4) M_1 + (C_1 D_2 D_4 - C_4 D_1 D_2) M_3 + (C_3 D_1 D_2 - C_1 D_2 D_3) M_4) \\ + (e^{nh_3} ((C_2 D_3 D_4 - C_4 D_2 D_3) M_1 + (C_4 D_1 D_3 - C_1 D_3 D_4) M_2 + (C_1 D_2 D_3 - C_2 D_1 D_3) M_4) \\ + (e^{nh_4} ((C_3 D_2 D_4 - C_2 D_3 D_4) M_1 + (C_1 D_3 D_4 - C_3 D_1 D_4) M_2 + (C_2 D_1 D_4 - C_1 D_2 D_4) M_3)) \} \sin(\xi x) \sin(\xi a_2 - \xi a_1) d\xi \quad (B1)$$

$$\begin{aligned}
k(x, t) = & \int_0^{\infty} \frac{\xi^{\kappa_1 - 1}}{2\Delta\mu_0} \{ e^{h(n_1+n_2)} ((C_2D_1D_4 - C_1D_2D_4)M_3 + (C_1D_2D_3 - C_2D_1D_3)M_4) \\
& + e^{h(n_1+n_3)} ((C_1D_3D_4 - C_3D_1D_4)M_2 + (C_3D_1D_2 - C_1D_2D_3)M_4) \\
& + e^{h(n_1+n_4)} ((C_4D_1D_3 - C_1D_3D_4)M_2 + (C_1D_2D_4 - C_4D_1D_2)M_3) \\
& + e^{h(n_2+n_3)} ((C_3D_2D_4 - C_2D_3D_4)M_1 + (C_2D_1D_3 - C_3D_1D_2)M_4) \\
& + e^{h(n_2+n_4)} ((C_2D_3D_4 - C_4D_2D_3)M_1 + (C_4D_1D_4 - C_2D_1D_4)M_3) \\
& + e^{h(n_3+n_4)} ((C_4D_2D_3 - C_3D_2D_4)M_1 + (C_3D_1D_4 - C_4D_1D_3)M_3) - \frac{(\kappa_1 + 1)}{8\mu_0} \} \sin(\xi(x-t)) d\xi
\end{aligned} \tag{B2}$$

$$\begin{aligned}
\Delta = & e^{h(n_1+n_2)} (C_1C_3D_2D_4 - C_1C_4D_2D_3 - C_2C_3D_1D_4 - C_2C_4D_1D_3) \\
& + e^{h(n_1+n_3)} (-C_1C_2D_3D_4 + C_1C_4D_2D_3 + C_2C_3D_1D_4 - C_3C_4D_1D_2) \\
& + e^{h(n_1+n_4)} (C_1C_2D_3D_4 - C_1C_3D_2D_4 - C_2C_4D_1D_3 + C_3C_4D_1D_2) \\
& + e^{h(n_2+n_3)} (C_1C_2D_3D_4 - C_1C_3D_2D_4 - C_2C_4D_1D_3 + C_3C_4D_1D_2) \\
& + e^{h(n_2+n_4)} (-C_1C_2D_3D_4 + C_1C_4D_2D_3 + C_2C_3D_1D_4 - C_3C_4D_1D_2) \\
& + e^{h(n_3+n_4)} (C_1C_3D_2D_4 - C_1C_4D_2D_3 - C_2C_3D_1D_4 + C_2C_4D_1D_3)
\end{aligned} \tag{B3}$$